# Surface structure of *i*-$Al_{68}Pd_{23}Mn_9$: An analysis based on the $\mathcal{T}^{*(2F)}$ tiling decorated by Bergman polytopes

G. Kasner
*Institut für Theoretische Physik, Universität Magdeburg, PSF 4120, D-39016 Magdeburg, Germany*

Z. Papadopolos and P. Kramer
*Institut für Theoretische Physik, Universität Tübingen, Auf der Morgenstelle 14, D-72076 Tübingen, Germany*

D. E. Bürgler
*Institut für Physik, Universität Basel, Klingelbergstrasse 82, CH-4056 Basel, Switzerland*
(Received 6 July 1998; revised manuscript received 16 October 1998)

A Fibonacci-like terrace structure along a fivefold axis of *i*-$Al_{68}Pd_{23}Mn_9$ monograins has been observed by Schaub *et al.* with scanning tunneling microscopy. In the planes of the terraces they see patterns of dark pentagonal holes. These holes are well oriented both within and among terraces. In one of 11 planes Schaub *et al.* obtain the autocorrelation function of the hole pattern. We interpret these experimental findings in terms of the $\mathcal{T}^{*(2F)}$ tiling decorated by Bergman and Mackay polytopes. Following the suggestion of Elser that the Bergman polytopes, clusters are the dominant motive of this model, we decorate the tiling $\mathcal{T}^{*(2F)}$ with the Bergman polytopes only. The tiling $\mathcal{T}^{*(2F)}$ allows us to use the powerful tools of the projection techniques. The Bergman polytopes can be easily replaced by the Mackay polytopes as the only decoration objects, if one believes in their particular stability. We derive a picture of ''geared'' layers of Bergman polytopes from the projection techniques as well as from a huge patch. Under the assumption that no surface reconstruction takes place, this picture explains the Fibonacci sequence of the step heights as well as the related structure in the terraces qualitatively and to a certain extent even quantitatively. Furthermore, this layer picture requires that the polytopes are cut in order to allow for the observed step heights. We conclude that Bergman or Mackay clusters have to be considered as geometric building blocks (just the polytopes) of the *i*-Al-Pd-Mn structure rather than as energetically stable entities (clusters). [S0163-1829(99)02829-5]

## I. INTRODUCTION

The surface of *i*-$Al_{68}Pd_{23}Mn_9$ perpendicular to fivefold axes of an icosahedron has been explored in various papers, and terraces similar to netplanes in crystals have been observed.[1] Schaub *et al.*[1] obtained by scanning tunneling microscopy (STM) atomic-scale direct space information and low-energy electron diffraction (LEED) patterns of the sputtered and annealed quasicrystalline surface. The dynamical LEED study of Gierer *et al.*[2] of a similarly prepared surface confirmed the quasicrystalline structure and yielded additional structural information allowing an identification of the possible surface layers in terms of the bulk structure model by de Boissieu *et al.*[3]

A second STM study of *in situ* cleaved surfaces by Ebert *et al.*[4] revealed terraces orthogonal to the fivefold direction only after annealing of the initially rather rough surface orthogonal to the twofold direction.

For the bulk structure of *i*-Al-Pd-Mn there exists a model due to de Boissieu *et al.*, see Ref. 3 and the references quoted within. This structure was based on the geometric model applied already on *i*-Al-Cu-Fe by Katz and Gratias, see Ref. 5 and the references within. The model has been generalized by Elser[6] into the geometric model that we reinterpreted as the particular decoration of the tiling $\mathcal{T}^{*(2F)}$.[7,8] We are interested for the geometric description, because the experimental STM measurements[1] are also giving only the geometric description, and we consider the geometric model as a model for the *atomic positions*, independently of the particular chemical identity of the atoms (Al, Pd, or Mn) occupying these positions. Therefore, all our conclusions will be valid for both the de Boissieu–Boudard model[3] and the Elser model[6] with the particular decoration of the atomic positions by Al, Pd, and Mn. The geometric model[6] consists of alternating Bergman and Mackay polytopes on the vertices of the primitive tiling.[9] Elser proposed that the Bergman polytopes are not only *geometric clusters*, polytopes, but should also be considered as *energetically stable clusters*. Our considerations are testing the conjecture.

We interpret the geometric model as the tiling $\mathcal{T}^{*(2F)}$ (Ref. 7) decorated by Bergman polytopes and some other, additional atomic positions (see Ref. 8 and Sec. III) forming Mackay polytopes. As suggested by Elser,[6] the dominant motives on this tiling model are dodecahedral Bergman clusters. We adopt this suggestion (neglecting the additional atomic positions) and examine the layer stacking and the structure within planes perpendicular to a fivefold axis. We compare the qualitative and quantitative predictions of the planar structure of the bulk model with the experimental findings at the surface.[1]

The model analysis is made in terms of a patch of the tiling $\mathcal{T}^{*(2F)}$ (Ref. 10) in the tenth step of inflation decorated by Bergman polytopes. This method allows us to generate the relevant planar structure orthogonal to a fivefold direction. By the method of lifting we can relate the planar patch structure in $\mathbb{E}_{\parallel}$ to the relevant triacontahedral window in $\mathbb{E}_{\perp}$ with its coding substructure for the tiling $\mathcal{T}^{*(2F)}$ and find in

 

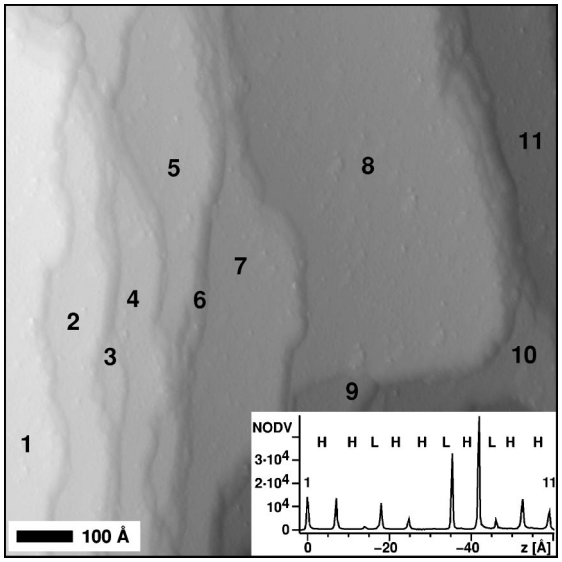


FIG. 1. The terrace structure of the $i$-$Al_{68}Pd_{23}Mn_9$ monograin (Ref. 1).

it the coding for the planes. An alternative approach to the terrace structure starting from the window side is given in Ref. 11.

## II. EXPERIMENT

The terrace structure of the $i$-$Al_{68}Pd_{23}Mn_9$ monograin has been observed by STM.[1] The terraces orthogonal to the five-fold axis are placed on Fibonacci distances with the short (low) interval $L=4.22\pm0.26$ Å and long (high) interval $H=6.78\pm0.24$ Å. The planes (as terraces) occur in the sequence H H L H H L H L H H, see Fig. 1.

In each plane there are dark pentagons (pentagonal holes) oriented parallel to each other, both in a terrace and among the terraces.[1] In the terraces there are also white five stars with five dark pentagons between the star arms, see Fig. 2.

In each plane one can draw lines through the structure

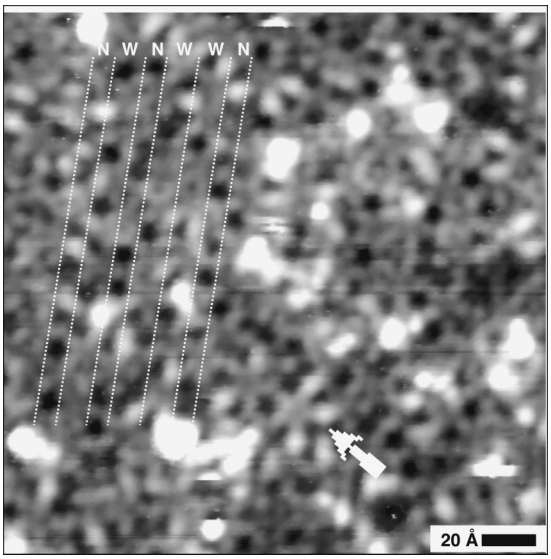


FIG. 2. Atomic-scale structure within the terraces (Ref. 1). Data taken on terrace 8 of Fig. 1. The white 5 star is marked by an arrow.

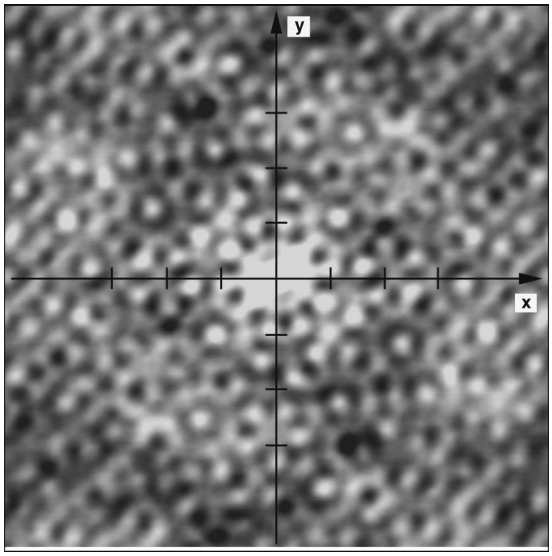


FIG. 3. Patterson distribution function of the pentagonal holes on terrace 8 (Ref. 1). The $x$ and $y$ axes extend from $-100$ to $+100$ Å.

such that they are on Fibonacci distances, short (narrow) $N=7.17\pm0.08$ Å and long (wide) $W=11.6\pm0.13$ Å. The short interval N equals the height of the pentagonal holes. The Patterson distribution function of the pentagonal holes in the biggest terrace (8) has been determined, see Fig. 3.

## III. GEOMETRIC MODEL FOR THE ATOMIC POSITIONS

In order to see if the geometric model of $i$-Al-Pd-Mn (Ref. 6) can explain the terrace structure, we consider this atomic model interpreted in terms of the canonical tiling $\mathcal{T}^{*(2F)}$,[7,8] see Fig. 4.

The tiling $\mathcal{T}^{*(2F)}$ is related[7] to the primitive tiling $\mathcal{T}^{P}$

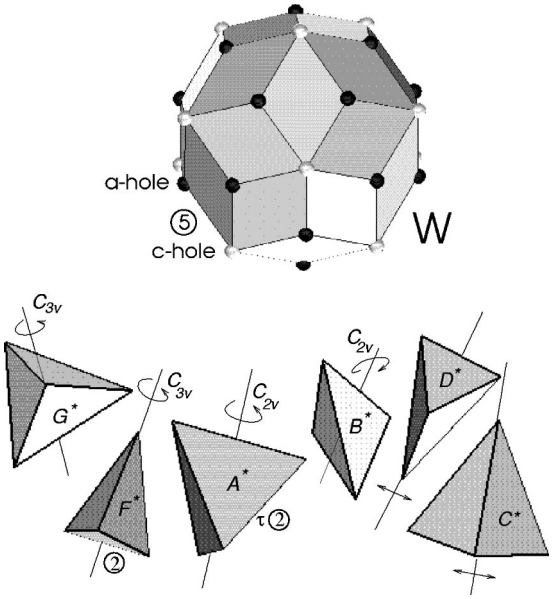


FIG. 4. The window of the tiling $\mathcal{T}^{*(2F)}$, is a triacontahedron, the six tetrahedra are the tiles (Ref. 7). The symbols ⑤ and ② are the standard lengths defined in Sec. III A.

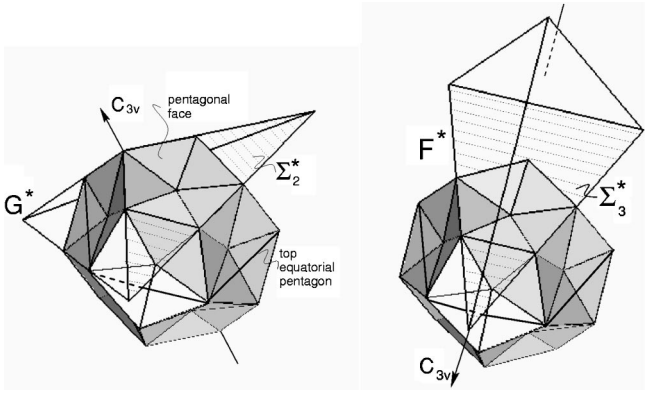


FIG. 5. The Bergman polytopes are typically hanging from the golden triangles $\Sigma_2^*$ and $\Sigma_3^*$ as the faces of the tiling $\mathcal{T}^{*(2F)}$. Pentagonal faces of the Bergman polytope (essentially a dodecahedron) and top equatorial pentagons, bigger by a factor $\tau$, are marked. Pentagonal faces and top pentagons of the hanging Bergman polytopes are drawn in Fig. 11, see also the black pentagons of the size of the top equatorial pentagons in Fig. 12.

(Ref. 9) by converting only the two (of six) tetrahedra $G^*$ ($G_\parallel^*$) and $F^*$ ($F_\parallel^*$) into acute and obtuse rhombohedra, respectively. The vertices of the tiling $\mathcal{T}^{*(2F)}$ then coincide with the *even vertices* (even index sum) of the primitive tiling. In the full geometric model, all the Mackay polytopes are centered on these vertices, although, not all these vertices are the centers of the Mackay polytopes. In the decoration of the tiling $\mathcal{T}^{*(2F)}$, Bergman polytopes (clusters) are centered[8] at the *odd vertices* (odd index sum) of the primitive tiling, which are *not* vertices of the tiling $\mathcal{T}^{*(2F)}$. It turns out that at least some pentagonal faces of each Bergman polytope (essentially a dodecahedron) appear in the tiling $\mathcal{T}^{*(2F)}$ inscribed in the faces $\Sigma_2^*$ ($\Sigma_{2\parallel}^*$) and $\Sigma_3^*$ ($\Sigma_{3\parallel}^*$) of the tetrahedra, as shown in Fig. 5 on an example of $G^*$ and $F^*$ tetrahedra. $\Sigma_2^*$ and $\Sigma_3^*$ are equilateral golden triangles *orthogonal* to the fivefold symmetry axes of an icosahedron. They are described in Sec. III A together with other geometric properties of the tiling $\mathcal{T}^{*(2F)}$.

### A. The planar structure of the tiling $\mathcal{T}^{*(2F)}$

We start with a description of the window in $\mathbb{E}_\perp$ for the tiling $\mathcal{T}^{*(2F)}$ and its coding content. The window for the tiling is a triacontahedron. Our aim is to look for a possible coding of the planes orthogonal to a fivefold direction of an icosahedron, that appear as a Fibonacci sequence on mutual distances as observed in the experiment.[1] These planes should contain the quasilattice points of $\mathcal{T}^{*(2F)}$. With respect to a fixed fivefold axis, we slice the triacontahedron into ten perpendicular zones of five types (1, 2, ... 5) as shown in Fig. 6. The thickness of unions of these zones is

$$
\begin{aligned}
1 = +1 \cup -1 = \pm 1 \equiv x = [2/(\tau+2)]\textcircled{5} \\
\pm 1 \cup \pm 2 = 1 \cup 2 = \tau x \\
\pm 1 \cup \pm 2 \cup \pm 3 = 1 \cup 2 \cup 3 = \tau^2 x \\
\pm 1 \cup \pm 2 \cup \pm 3 \cup \pm 4 \\
= 1 \cup 2 \cup 3 \cup 4 = \tau^3 x.
\end{aligned}
$$

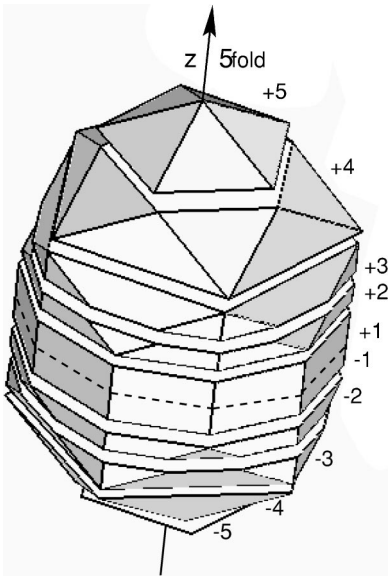


FIG. 6. The window (triacontahedron) sliced into ten perpendicular zones orthogonal to a fivefold axis. The point zero is at the center of the triacontahedron. With respect to this point zero, the zones are denoted by $\pm 1$, $\pm 2$, $\pm 3$, $\pm 4$, and $\pm 5$.

The symbol ⑤ is the standard distance $1/\sqrt{2}$ along a direction parallel to a fivefold symmetry axis of an icosahedron, $\tau=(1+\sqrt{5})/2$. The symbol ② is the standard distance $\sqrt{2/(\tau+2)}$ along a direction parallel to a twofold symmetry axis of an icosahedron; the relation in length to the standard ⑤ is ②$=2/(\sqrt{\tau+2})$ ⑤.

Considering the thickness of zones and their combinations we look for windows that would be necessary to code Fibonacci sequences of planes perpendicular to the fivefold axis. The decagonal middle zone of type 1 (decagonal prism) is the window[7] for the canonical planar tiling $\mathcal{T}^{*(A_4)}$ by two golden triangles.[12] This fact has been denoted as the dissectability of the $\mathcal{T}^{*(2F)}$ into planar subtilings $\mathcal{T}^{*(A_4)}$.[7] The thickness $x$ of the zone 1 (the decagonal prism) allows, as a necessary condition, for coding a Fibonacci sequence of planes with mutual distances in $\mathbb{E}_\parallel$ $s \equiv s_\parallel = \tau^3(2/(\tau+2))$⑤ and $l \equiv l_\parallel = \tau s$

$$x = |s_\perp| + |l_\perp|,$$

where $x$ is to be understood as a window.[10] The thicknesses for the unions of the zones $1 \cup 2$, $1 \cup 2 \cup 3$, and $1 \cup 2 \cup 3 \cup 4$ scale this window by up to three powers of $\tau$. Consequently they may code the Fibonacci sequences of planes in $\mathbb{E}_\parallel$ three times inflated, respectively. The final sequence consists of mutual distances $s=[2/(\tau+2)]$⑤ and $l=\tau s$.

The significance of the zones in the tiling is related to their content of windows for geometric objects other than quasilattice points: the 1D edges of the tiling have as windows the perpendicular projections of dual 5 boundaries, and the faces of the tiling the perpendicular projections of dual 4 boundaries. We consider the edges and the faces of the tiling $\mathcal{T}^{*(2F)}$ in the planes perpendicular to a fixed direction of a fivefold axes. They are coded by the corresponding dual boundaries related to the same fivefold axes in $\mathbb{E}_\perp$. In these planes there can appear only two of the four kinds of faces of the tiling, the golden triangles $\Sigma_{2\parallel}^*$ and $\Sigma_{3\parallel}^*$. They are equi-

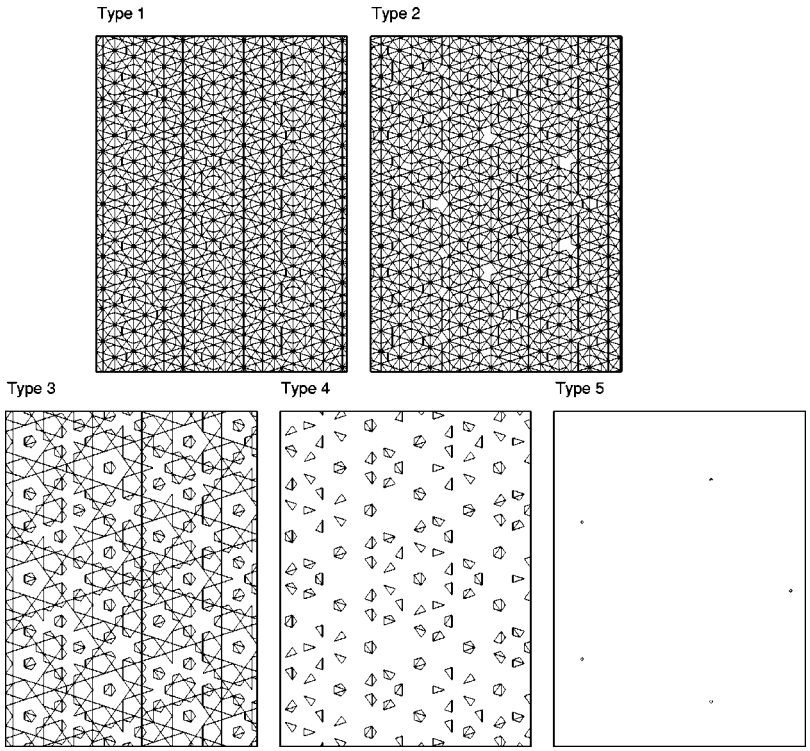


FIG. 7. Examples in $\mathbb{E}_\parallel$ of the planar sections orthogonal to the fivefold axis of the tiling $\mathcal{T}^{*(2F)}$, such that the planes contain quasilattice points, the tiling vertices. Types 1–5 are coded in the window by the corresponding zones $\pm 1, \pm 2, \ldots, \pm 5$, see Fig. 6. The golden triangles $\Sigma^*_{2\parallel}$ and $\Sigma^*_{3\parallel}$ (see also Fig. 5) define the structure of planes of types 1–4.

lateral triangles with one edge $\tau$② and two edges ②, and one edge ② and two edges $\tau$②, respectively. They are coded by the 4 boundaries projected to $\mathbb{E}_\perp$, $\Sigma_{2\perp}$, and $\Sigma_{3\perp}$, respectively.[7] Similarly the short edge ②$=\Omega^*_{1\parallel}$ and the long edge $\tau$②$=\Omega^*_{2\parallel}$ of these two triangles have the windows $\Omega_{1\perp}$ and $\Omega_{2\perp}$, respectively.[7] All the points of these projected dual boundaries, related to the particular fivefold direction, are located within the triacontahedron and moreover inside the union $1\cup 2\cup 3\cup 4$ and not in the zone 5. From their intersections with the first decagonal prism we get the full coding for the triangle pattern $\mathcal{T}^{*(A_4)}$ in $\mathbb{E}_\parallel$. For zones 2, 3, and 4 outside the decagonal prism we expect in $\mathbb{E}_\parallel$ a gradual reduction in the density of triangle faces and edges, due to the disappearance of their coding in the zones. We also expect qualitative differences in the pattern in the planes of different types. Finally, in zone 5 we expect no such triangles and edges. These reductions should go along with a reduction of the density of quasilattice points for the tiling $\mathcal{T}^{*(2F)}$.

Here we do not prove the sufficient condition for the existence of Fibonacci sequences of planes. In Ref. 11 we identify the vectors which generate this Fibonacci sequence. Instead we check our expectations based on the necessary conditions from the side of the window on the finite patch in $\mathbb{E}_\parallel$ obtained by the inflation procedure for the tiling $\mathcal{T}^{*(2F)}$.[10] We inspect a ten-step inflation patch. We cut the patch of $\mathcal{T}^{*(2F)}$ in $\mathbb{E}_\parallel$ by planes orthogonal to the fivefold direction whenever there is a quasilattice point. There appear 318 planes on three mutual distances: $\tau^{-1}[2/(\tau+2)]$⑤, $[2/(\tau+2)]$⑤ and $\tau[2/(\tau+2)]$⑤. The patch construction will allow us to simulate in detail the planar structure and its sequence and to compare it with experimental findings.[1]

At the same time we wish to keep track of the coding window structure described above. For this purpose we pass to $\mathbb{E}_\perp$ by the unique procedure of lifting the quasilattice points of the patch into the triacontahedral window. The points within each plane of $\mathbb{E}_\parallel$ perpendicular to a fivefold axis are lifted into an intersection of the triacontahedron with a plane shifted along and perpendicular to the corresponding five axis in $\mathbb{E}_\perp$. From the shift (with respect to the center of all the points of the patch), we assign to each plane one of the ten zones $\pm 1$, $\pm 2$, $\pm 3$, $\pm 4$, $\pm 5$ of the triacontahedron introduced before. In the generated patch there appear five families of planes in $\mathbb{E}_\parallel$, corresponding to the ten zones of five types in $\mathbb{E}_\perp$: The decagonal prism yields the densest planes with the golden triangle tiling. Zones 2, 3, and 4 give planes still containing golden triangles (and edges) of the triangle tiling. In contrast, the planes in $\mathbb{E}_\parallel$ of type 5 in $\mathbb{E}_\perp$ contain only points of the quasilattice but neither edges nor faces (see Fig. 7). In the patch, there are 234 planes of the types $1\cup 2\cup 3\cup 4$ and they do appear in a Fibonacci sequence with a short $s$ and a long $l$ spacing. As expected $s \equiv s_\parallel = [2/(\tau+2)]$⑤, $l \equiv l_\parallel = \tau[2/(\tau+2)]$⑤; $|s_\perp| + |l_\perp| = \tau^3 x$, where $\tau^3 x$ is the thickness of the window for the Fibonacci spacing. Also the types $1\cup 2\cup 3$, $1\cup 2$, and 1 appear in corresponding by $\tau$, $\tau^2$, and $\tau^3$, respectively, inflated Fibonacci sequences. Finally, the planes of type 5 are not part of the Fibonacci sequence, and lead to the three distances among the planes of *all* types, $\tau^{-1}[2/(\tau+2)]$⑤, $[2/(\tau+2)]$⑤ and $\tau[2/(\tau+2)]$⑤. The planes of type 5 carry a low density of quasilattice points.

In the geometric model under consideration the scale is $\tau$ times bigger than in $\mathcal{T}^{*(2F)}$.[8] The short edge has length $\tau$② and the long edge $\tau^2$②. For *i*-Al-Pd-Mn, the standard length

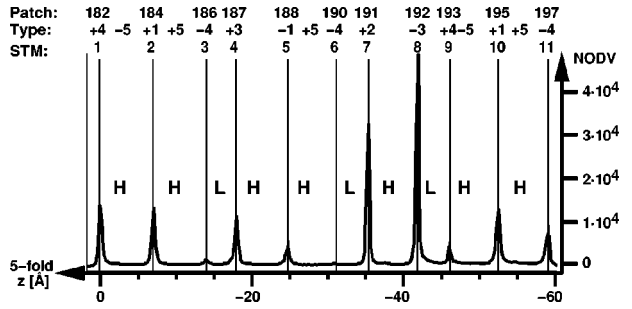


FIG. 8. In the ten-times inflated patch we find a sequence that corresponds to the 11 terraces observed by STM. The plot shows a histogram of Fig. 1 (NODV is the number of data values). The numbers and types (zones) of the planes in the patch and the number of the corresponding terrace in the STM image (Fig. 1) are indicated above the plot. Note that the planes of types $\pm 5$ are not observed in the experiment.

is ⑤$=4.56$ Å.[3] Inserting it into the model the two spacings of the planes $1 \cup 2 \cup 3 \cup 4$ become $\tau s \equiv L = \tau[2/(\tau+2)]$⑤ $=4.08$ Å and $\tau l \equiv H = \tau^2[2/(\tau+2)]$⑤$=6.60$ Å, in agreement with the measured step heights.[1]

### B. The layers of the Bergman polytopes related to the planes of the $\mathcal{T}^{*(2F)}$ tiling

In the 10 times inflated patch we find 20 sequences of 11 planes such that each sequence could correspond to the observed 11 terraces in the experiment[1] on the distances H H L H H L H L H H, see Fig. 1. Let us take one of these sequences, the one from 182–197 and plot it along the sequence determined by the experiment, Fig. 8. In the sequence 182–197 there are five planes of type 5 that are not observed in the measurement. The biggest terrace observed in the experiment, denoted by the number 8 (Ref. 1), appears to correspond to plane 192 of type 3 in the sequence. In our 20 sequences, on the position of plane 8 there appears 16 times the plane of type 3, coded in the zone $-3$, and four times of type 2, coded in the zone $-2$. For all 20 sequences the first plane is of type 4, coded in the zone $+4$ by the interval $[\min(z_\perp), \max(z_\perp)] \sim (0.681, 0.825)$. The whole zone $+4$ is coded by the interval $(\tau^3 x/2, \tau^2 x/2) \sim (0.828, 0.521)$. The coding interval of the plane equivalent to terrace 8 is $(-0.434, -0.290) \subset (-\tau^2 x/2, -x/2)$.

So far we considered the points, edges, and faces of the tiling in the sequence of planes orthogonal to a fivefold direction. Now we turn to the decoration by the Bergman clusters, as suggested by Elser.[6] The decoration of the tiling

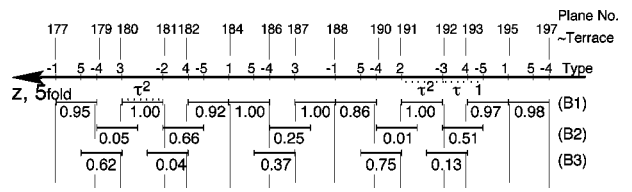


FIG. 9. All layers of Bergman polytopes orthogonal to a fivefold direction ($z$ axis) in a part of the ten-step inflation patch containing the planes 177–197. The dotted intervals mark the relative distances between the planes and the height of the Bergman polytopes. The height of the Bergman polytope equals the length $H$, where $H=6.60$ Å. In the figure $H \sim \tau^2$.

TABLE I. The densities of the quasilattice points $q$, $\rho(q)$ of the tiling $\mathcal{T}^{*(2F)}$ in planes 177–197 of the ten-times inflated patch. $\rho(q)$ is normalized with respect to planes coded by the decagonal prism in triacontahedron. The symbol $\eta$ is the normalized $z$ coordinate in $\mathbb{E}_\perp$, $\eta = z/(\tau$ ⑤$)$, the coordinate of the plane–coding in the window for $\mathcal{T}^{*(2F)}$, is $\eta \in (-1,1)$. $\rho_b(B)$ and $\rho_a(B)$ are, respectively, the densities of the Bergman-polytope layers below and above the planes with respect to the direction of the $z$ axis in $\mathbb{E}_\parallel$. $\rho(B)$ are normalized with respect to the layers with the maximal density (see Ref. 11, where the meaning of the expected sharp values 0 and 1 in the brackets is explained). The corresponding 11 terraces are situated between planes 182 and 197 as in Fig. 8.

| Plane | Type | $\eta(q)$ | $\rho(q)$ | $\rho_b(B)$ | $\rho_a(B)$ |
|---|---|---|---|---|---|
| 177 | $-1$ | $-0.050$ | 1.00 | 0.95 | 0.99 |
| 178 | 5 | 0.845 | 0.10 | 0.62 | 0.00 (0) |
| 179 | $-4$ | $-0.603$ | 0.55 | 0.05 | 0.95 |
| 180 | 3 | 0.292 | 0.97 | 1.00 (1) | 0.62 |
| 181 | $-2$ | $-0.261$ | 0.98 | 0.66 | 1.00 (1) |
| 182 | 4 | 0.633 | 0.51 | 0.92 | 0.04 |
| 183 | $-5$ | $-0.814$ | 0.13 | 0.00 (0) | 0.66 |
| 184 | 1 | 0.081 | 1.00 | 1.00 | 0.92 |
| 185 | 5 | 0.975 | 0.00 | 0.37 | 0.00 (0) |
| 186 | $-4$ | $-0.472$ | 0.76 | 0.25 | 1.00 |
| 187 | 3 | 0.422 | 0.85 | 1.00 (1) | 0.37 |
| 188 | $-1$ | $-0.131$ | 1.00 | 0.86 | 1.00 |
| 189 | 5 | 0.764 | 0.23 | 0.75 | 0.00 (0) |
| 190 | $-4$ | $-0.683$ | 0.39 | 0.01 | 0.86 |
| 191 | 2 | 0.211 | 0.99 | 1.00 (1) | 0.75 |
| 192 | $-3$ | $-0.342$ | 0.92 | 0.51 | 1.00 (1) |
| 193 | 4 | 0.553 | 0.66 | 0.97 | 0.13 |
| 194 | $-5$ | $-0.894$ | 0.04 | 0.00 (0) | 0.51 |
| 195 | 1 | 0.000 | 1.00 | 0.98 | 0.97 |
| 196 | 5 | 0.894 | 0.05 | 0.53 | 0.00 (0) |
| 197 | $-4$ | $-0.553$ | 0.64 | 0.10 | 0.98 |

$\mathcal{T}^{*(2F)}$ by the Bergman polytopes is performed as stated in Sec. III A, and Ref. 8. As a final result, related to the planes of type 1–5 orthogonal to a fivefold axes, there appear *layers* of Bergman polytopes. The edge of the Bergman polytope (dodecahedron) is $\tau^{-1}$②$=2.96$ Å and consequently the height of the dodecahedron, and the layers, is $\tau^2[2/(\tau+2)]$⑤$=6.60$ Å. It equals the high spacing of the Fibonacci planes of type 1–4, $H=6.60$ Å.

In Fig. 9 all layers of Bergman polytopes with two opposite pentagonal faces orthogonal to a fivefold direction ($z$ axis) in a part of the ten-step inflation patch are presented. Part of the patch contains the planes 177–197, such that it includes 11 planes from Fig. 8. The length of horizontal lines in the rows (B1), (B2), (B3) represents the height of a Bergman dodecahedron, and their horizontal positions give the positions with respect to quasilattice planes. Horizontal lines to the right of a quasilattice plane denote Bergman polytopes hanging below the plane, and horizontal lines to the left are Bergman polytopes standing on the plane. In particular, (B1) are the layers of Bergman polytopes such that they are in between the planes of type $\pm 1, \pm 2, \pm 3, \pm 4$, hanging from one plane and standing on another. (B2) are the layers of Bergman polytopes hanging from some of the planes of type $\pm 1, \pm 2, \pm 3, \pm 4$ and eventually standing on a plane of type

5. (B3) are the layers of Bergman polytopes standing on some of the planes of type $\pm 1, \pm 2, \pm 3, \pm 4$ and eventually hanging on a plane of type 5. Hence, the latter cannot be interpreted as situated below any of the planes of type $\pm 1$, $\pm 2, \pm 3, \pm 4$ . The densities of all the layers, $\rho(B)$ $[\rho_b(B), \rho_a(B)]$ are written in Fig. 9 under the horizontal lines representing Bergman layers, see also Table I. The layers of Bergman polytopes are ''geared'' to each other.

If we wish to interpret the observed terraces as the planes of types 1–4 and consider the Bergman polytopes as the clusters,[6] then we relate to each terrace (plane) the layer of the Bergman polytopes *below* the plane, i.e., the layer of hanging Bergman clusters. These clusters touch with a pentagonal face a plane of quasilattice points from below. If that happens, the atomic position at the midpoint of the face is lowered with respect to the plane by 0.48 Å, occupied by Al in the $B_5$ position of the model.[3] This face could appear as a dark hole in the STM experiment. The search for these pentagonal faces within the planes of types 1–4 is equivalent to the search for those Bergman clusters which hang below these planes (from layers B1 and B2). Knowing the coding interval in the window for terrace 8, $(-0.434, -0.290) \subset (-\tau^2 x/2, -x/2)$, one can, as shown in Ref. 11, compute the density of the corresponding hanging Bergman polytope layer. Using this approach we find the density of terrace 8 to be in the range of $5.72–8.62 \times 10^{-3}$ hanging Bergman clusters/Å $^2$.

As we already stated, the planes of types 1–4 are by their mutual distances in agreement with the terraces observed by STM.[1] The planes of type 5 are not observed as terraces, probably due to the low densities of the quasilattice points in the planes. How is the appearance of the terraces related to the Bergman layers? The planes as terraces appear to be correlated to two or three Bergman layers such that one layer is above the plane, another below the plane, and the eventual third one is dissected by the plane. These planes are of types 1–4. For planes which appear correlated to only two Bergman layers such that, with respect to the previous case, either the layer above or below the plane is missing, a terrace does not appear. These planes are of type 5.

### C. Interpretation of the pentagonal holes in the planes

The observed dark pentagonal holes[1] of the estimated height $7.17 \pm 0.08$ Å are approximately $\tau$ times bigger than the pentagonal faces (face pentagons, see Fig. 5) of the Bergman polytopes. The height of the Bergman face within the plane is 4.56 Å. The observed pentagonal holes are as big as the pentagons on a parallel cut through five vertices of the dodecahedron with identical orientation, see Fig. 5. Their height is 7.38 Å. We call them top equatorial pentagons. Such a pentagonal cut through a Bergman cluster would again have a midpoint, in this case lowered by 0.78 Å, occupied by Pd according to the model.[3] Such a pentagon could also appear as a hole. The planes in the tiling and in the patch which contain these top equatorial pentagons are shifted with respect to the former planes by $[2/(\tau+2)]$⑤ $= 2.52$ Å. Tentatively we propose this alternative interpretation of the pentagonal holes in the planes. The identification of the pentagonal holes as top equatorial pentagons of Bergman polytopes is appealing because it readily explains the size of the pentagons. However, there is a disagreement with the separation of the two topmost layers determined in a LEED-IV analysis by Gierer *et al.*[2] They find a separation of 0.38 Å, which is interpreted as a contracted bulk layer separation of 0.48 Å. This value, in turn, would nicely fit the depth of the Bergman ''faces.'' Therefore, a clearcut interpretation of the pentagons observed by STM is still lacking.

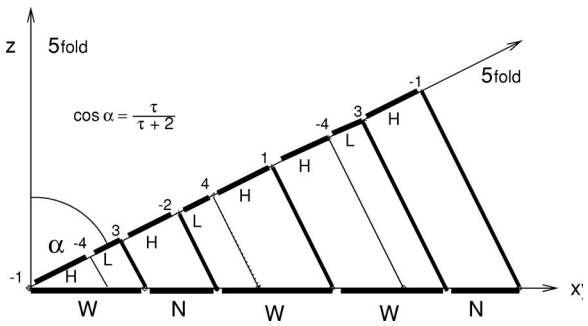


FIG. 10. Possible relation of the Fibonacci spacings of the planes (terraces) of type 1–3 with the Fibonacci spacings of the lines in the planes based on the $\mathcal{T}^{*(2F)}$ tiling.

It is important to note that if we wish to relate the experimental data with the geometric model,[6,8] this implies in any case that the Bergman polytopes of height $\tau^2[2/(\tau+2)]$⑤ $= 6.60$ Å are cut by the terrace structure with a minimal layer separation of 4.22 Å, see Fig. 9.

The Mackay polytopes of the full geometric model[6,8] would also provide pentagonal holes. Their height would be 7.38 Å, but they are much deeper (2.52 Å), and Mn atoms on $M_0$ positions should be in the center.[3]

The lines analyzed in Ref. 1 in a fixed plane with pentagons (see Fig. 2) can be understood in the model as follows: Take another fivefold axis at an angle $\alpha$ (see Fig. 10), $\cos\alpha = \tau/(\tau+2) = 1/\sqrt{5}$ with respect to the fixed one (chosen as $z$ axes) and consider its set of planes of type $1 \cup 2 \cup 3$. These planes will intersect the fixed plane in parallel lines in Fibonacci spacing with distances N and W, where $N = (\sqrt{5}/2)H = 7.38$ Å and $W = (\sqrt{5}/2)(L+H) = 11.94$ Å, $\sin\alpha = 2/\sqrt{5}$, see Fig. 10. These distances compare well with the experiment.[1]

From Fig. 8 we see that terrace 8, on which the Patterson distribution function of the pentagonal holes (Figs. 2 and 3) was determined,[1] corresponds to plane 192 in the sequence of planes 182–197 of the ten-times inflated patch.

In Fig. 11 only those golden triangles of plane 192 are presented, from which Bergman polytopes are hanging. They are hanging with respect to the positive direction of the $z$ axis of Figs. 8 and 9. These Bergman polytopes are placed between planes 192 and 194, below 192 and above 194.

In Fig. 12 we show the patterns of the top equatorial pentagons of Bergman polytopes in planes 188, 190, 191, and 192. These planes represent terraces 5, 6, 7, and 8, respectively. The pentagons are oriented parallel to each other, both in a terrace and among the terraces, as observed in Ref. 1. Big fluctuations in the density of the Bergman polytopes in the layers is expected, see also Table I.

In order to compare our model to the experimentally obtained results on the distribution of the dark pentagonal holes in the STM measurement, we calculate the autocorrelation function (ACF) or Patterson function

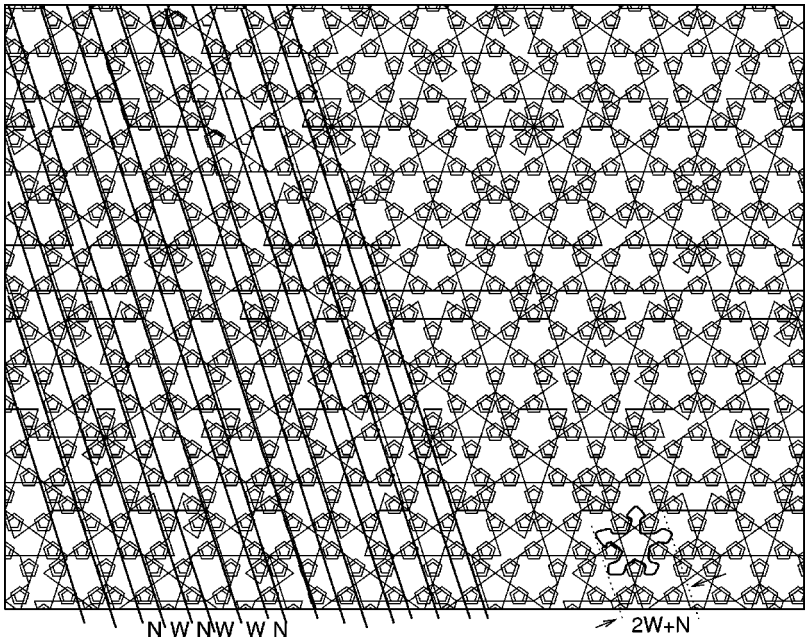


FIG. 11. The representation of terrace 8 by plane 192 of the ten-times inflated $\mathcal{T}^{*(2F)}$ patch. Note the pentagonal faces or $\tau$ bigger top equatorial pentagons of Bergman polytopes, hanging in the direction orthogonal to the plane, the lines on N and W distances (see Fig. 10), and the white star of height 2W+N. Compare to Fig. 2.

$$A(\vec{r}) = \int_{\mathcal{F}} z_h(\vec{r'}) z_h(\vec{r'} + \vec{r}) d^2 r',$$

where $\vec{r} = (x,y)$ and $z_h(\vec{r})$ denotes the hole image. The ACF for the distribution of the dark pentagons was calculated by digitizing plane 192 of the model in exactly the same manner as described in Ref. 1 by assigning the value 1 to those parts of the plane inside a pentagon and 0 otherwise. The resolution was also chosen to coincide with the one used in Ref. 1, namely 0.5 Å per pixel. Numerically we obtained the ACF for plane 192 of size $764 \times 764$ Å$^2$. The layer below plane 192 in the patch contains 3835 hanging Bergman polytopes and hence, the density of the pentagons in plane 192 is $6.58 \times 10^{-3}$ Å$^{-2}$. With respect to noise in the STM images, local-density fluctuations in small patches of a quasiperiodically decorated plane, and freedom in the choice of the grey-scale level (which separates between black and white in the digitizing procedure of the STM pattern), the estimated density on terrace 8 of $4.22 \times 10^{-3}$ Å$^{-2}$ can be considered to be in rather good agreement with that obtained from our model. The minimal distance between the pentagons equals the short edge of the tiling $\mathcal{T}^{*(2F)}$. In the geometric model[6,8] it equals $\tau ② = r_{\mathrm{calc}}(I') \approx 7.8$ Å. The mean distance for the pentagons in plane 192 is calculated to 12.33 Å. In Fig. 13 the resulting ACF is shown for a range of the displacement vectors of $\pm 100$ Å in $x$ and $y$ directions. Labels on the first ten maxima are in correspondence with those of Fig. 4 in Ref. 1 and Table II. The calculated peak positions fit well to those obtained from the hole pattern extracted from STM measurement, see Fig. 3 and Table II. The most intensive peak is the one marked by II in Fig. 13 and Table II, in the reasonable agreement with the Fig. 3. Instead of the series of planes on Fibonacci distances that we have studied in Sec. III A, from which the layers of Bergman polytopes are hanging, see Sec.

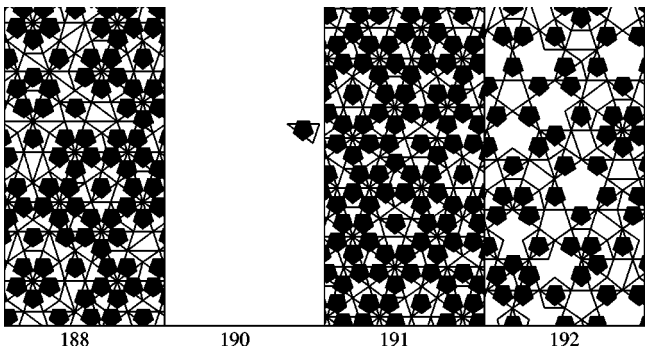


FIG. 12. The representation of terraces 5, 6, 7, and 8 by planes 188, 190, 191, and 192, respectively. The content are the golden triangles and the top equatorial pentagons of the Bergman polytopes.

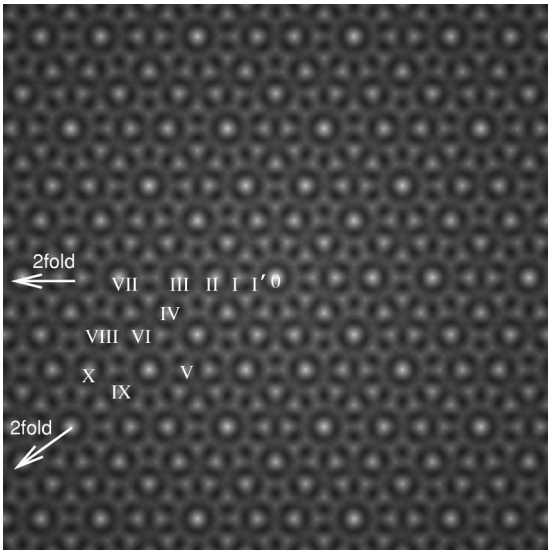


FIG. 13. The Patterson distribution function (the correlation maxima) of the pentagonal holes in plane 192. Compare to Fig. 3.

TABLE II. Radii of the Patterson correlation maxima in Fig. 3 $r_{exp}$ and in Fig. 13 $r_{calc}$.

| | 0 | I′ | I | II | III | IV | V | VI | VII | VIII | IX | X |
|---|---|---|---|---|---|---|---|---|---|---|---|---|
| $r_{exp}$(Å) | 0 | | ≈12 | 19.7 | 31.7 | 36.9 | 41.3 | 49.4 | 51.0 | 60.5 | 63.3 | 68.1 |
| $r_{calc}$(Å) | 0 | 7.8 | 12.6 | 20.3 | 32.9 | 38.6 | 43.7 | 50.7 | 53.2 | 62.5 | 65.7 | 66.7 |

III B, we could have found the Fibonacci sequence of the Bergman layers themselves.[11] In this frame, to terrace 8 would correspond the layer of Bergman polytopes hanging from Plane 195 with a much higher density of the Bergman polytopes (pentagons) (0.89) than in plane 192 (0.51) presented in Fig. 11, see also Table I. The first strongest peak in the Patterson distribution for the penatogons in the layer would have been on the corresponding much shorter distance in disagreement with the STM measurement, see Fig. 3. Both concepts, the Fibonacci sequence of planes and the layers of Bergman polytopes hanging from these planes, seem to be of importance for the terrace structure of the surface.

## IV. DISCUSSION

In this paper we have used the projection tools related to tiling $\mathcal{T}^{*(2F)}$. We have refined the already known dissectability property[7,10] of the tiling $\mathcal{T}^{*(2F)}$ along the fivefold direction and have transferred this inherent property of the tiling into the layer structure of the geometric model.[6,8]

In addition, we have generated a huge patch of the tiling $\mathcal{T}^{*(2F)}$ by a highly nontrivial inflation procedure[10] to linear dimensions of about 750 Å. It is large enough to reproduce all statistical predictions about densities from the projection method as well as to contain inflation symmetries (tenth step of the inflation).

We do not consider the choice of the geometric model with the Bergman and Mackay polytopes[6,8] as a significant restriction because most of the results derived above will also hold for models with approximately the same size of windows, as for example, the model from Janot[13] that we have not yet considered. We have focused on the geometric model defined as a decoration of the tiling (primitive $\mathcal{T}^{P}$, or $\mathcal{T}^{*(2F)}$) because all powerful tools known from the projection methods are applicable.

## V. CONCLUSION

We prove that the experimentally observed succession of the step heights L (low) and H (high) along the fivefold axis ($z$ direction), which obeys the Fibonacci sequence, also exists in the patch of the geometric model.[6,8] Additionally, we relate this sequence to another Fibonacci sequence of the distances N (narrow) and W (wide) between lines within the planes ($x$-$y$ planes) of the terraces also found in experiments.[1]

The estimated coding of the observed finite Fibonacci subsequence along the fivefold direction restricts the choice of planes in the model which have to be compared with the experimentally analyzed terraces. Our model predicts big variations of the densities of quasilattice points (or equivalently pentagonal holes) among terraces which should be measurable in future high-quality STM images.

Our analysis shows that the geometric model[6,8] can be understood as being composed of ''geared'' layers of Bergman polytopes (Fig. 9). We relate sequences of these layers of Bergman polytopes to the observed terraces and derive the patterns of pentagons within the terraces. We calculate the densities of Bergman clusters (Table I) within the layers based on the knowledge of the window for the Bergman clusters[11] as well as using our huge patch (Fig. 9). The calculated pentagon distribution yields a reasonable mean density and good agreement of the Patterson data (Fig. 13, Table II). The direct space patterns even reproduce some structures (white 5 stars) observed on the surface of the terraces. Other features of the patterns (Figs. 11 and 12) should be observable in future high-quality STM images. Hence, we predict more detailed criteria to judge from STM data whether the geometric model[6,8] is realized or not.

If we assume that the surface of *i*-Al-Pd-Mn is not reconstructed with respect to the bulk, a fact that follows from the work of Gierer *et al.*,[2] then the Bergman polytopes represent a correct geometric decoration, but they may not be considered as energetically stable clusters. This follows from the picture of ''geared'' layers of Bergman polytopes presented in Fig. 9 which requires that Bergman clusters are cut in order to allow for the observed step heights (H and L). Further, from the alternating decoration with Bergman and Mackay polytopes of the primitive tiling[6] one can also easily conclude that the same model cannot be interpreted as the Mackay-cluster model either. Therefore, the Bergman and Mackay clusters have to be considered as geometric building blocks of the quasicrystalline structure rather than as energetically stable entities. Strictly speaking, we can draw this conclusion only for clusters at surfaces as the vacuum interface gives rise to surface energy. Its influence on the surface morphology is not easily predictable as surface energy contributions play an important role for the cluster stability, too. The determination of the different energy contributions is beyond the scope of this study which is based on geometric considerations. However, we hope that our work stimulates future investigations of the energetic stability of Bergman and Mackay polytopes in icosahedral quasicrystals and at their surfaces.

## ACKNOWLEDGMENTS

Financial support of the DFG is gratefully acknowledged by Z. Papadopolos and P. Kramer. Z. Papadopolos acknowledges support from the Center de Physique Théorique, CNRS, Marseille where part of this work was done. We would also like to thank the Geometry-Center at the University of Minnesota for making Geomview freely available, which proved to be a valuable tool throughout our work.

[1] T. M. Schaub, D. E. Bürgler, H.-J. Güntherodt, and J. B. Suck, Phys. Rev. Lett. **73**, 1255 (1994); T. M. Schaub, D. E. Bürgler, H.-J. Güntherodt, J. B. Suck, and M. Audier, Appl. Phys. A: Mater. Sci. Process. **61**, 491 (1995).

[2] M. Gierer, M. A. Van Hove, A. I. Goldman, Z. Shen, S.-L. Chang, C. J. Jenks, C.-M. Zhang, and P. A. Thiel, Phys. Rev. Lett. **78**, 467 (1997); M. Gierer, M. A. Van Hove, A. I. Goldman, Z. Shen, S.-L. Chang, P. J. Pinhero, C. J. Jenks, J. W. Anderegg, C.-M. Zhang, and P. A. Thiel, Phys. Rev. B **57**, 7628 (1998).

[3] M. de Boissieu, P. Stephens, M. Boudard, C. Janot, D. L. Chapman, and M. Audier, J. Phys.: Condens. Matter **6**, 10 725 (1994).

[4] Ph. Ebert, F. Yue, and K. Urban, Phys. Rev. B **57**, 2821 (1998).

[5] A. Katz and D. Gratias, in *Proceedings of the 5th International Conference on Quasicrystals*, edited by C. Janot and R. Mosseri (World Scientific, Singapore, 1995), pp. 164–167.

[6] V. Elser, Philos. Mag. B **73**, 641 (1996).

[7] P. Kramer, Z. Papadopolos, and D. Zeidler, in *Symmetry in Science V: Algebraic Structures, their Representations, Realizations and Physical Applications*, edited by B. Gruber and L. C. Biedenharn (Plenum, New York, 1991), pp. 395–427; P. Kramer and Z. Papadopolos, Can. J. Phys. **72**, 408 (1994).

[8] P. Kramer, Z. Papadopolos, and W. Liebermeister, in *Proceedings of the 6th International Conference on Quasicrystals, Yamada Conference XLVII*, edited by S. Takeuchi and T. Fujiwara (World Scientific, Singapore, 1998), pp. 71–76; Z. Papadopolos, P. Kramer, and W. Liebermeister, in *Proceedings of the International Conference on Aperiodic Crystals, Aperiodic 1997*, edited by Marc de Boissieu, Jean-Louis Verger-Gaugry, and Roland Currant (World Scientific, Singapore, 1998), pp. 173–81.

[9] P. Kramer and N. Neri, Acta Crystallogr., Sect. A: Found. Crystallogr. **40**, 580 (1984).

[10] C. Hohneker, P. Kramer, and Z. Papadopolos, in *GROUP21 Physical Applications and Mathematical Aspects of Geometry, Groups, and Algebras, Vol. 2*, edited by H.-D. Doebner, W. Scherer, and C. Schulte (World Scientific, Singapore, 1997), pp. 982–986; Z. Papadopolos, C. Hohneker, and P. Kramer, Discrete Mathematics (to be published).

[11] P. Kramer, Z. Papadopolos, and H. Teuscher, J. Phys.: Condens. Matter **11**, 2729 (1999).

[12] M. Baake, P. Kramer, M. Schlottmann, and D. Zeidler, Int. J. Mod. Phys. B **4**, 2217 (1990).

[13] C. Janot, J. Phys.: Condens. Matter **9**, 1493 (1997).